The Astrophysical Journal Letters, 932:L2 (8pp), 2022 June 10 https://doi.org/10.3847/2041-8213/ac7235

A Speed Bump: SN 2021aefx Shows that Doppler Shift Alone Can Explain Early Excess Blue Flux in Some Type Ia Supernovae

C. Ashall[1], J. Lu[2], B. J. Shappee[1], C. R. Burns[3], E. Y. Hsiao[2], S. Kumar[2], N. Morrell[4], M. M. Phillips[4], M. Shahbandeh[2], E. Baron[5,6,7], K. Boutsia[4], P. J. Brown[8], J. M. DerKacy[5], L. Galbany[9,10], P. Hoeflich[2], K. Krisciunas[8], P. Mazzali[11], A. L. Piro[3], M. D. Stritzinger[12], and N. B. Suntzeff[8]
[1] Institute for Astronomy, University of Hawaii, 2680 Woodlawn Drive, Honolulu, HI 96822, USA; chris.ashall24@gmail.com
[2] Department of Physics, Florida State University, 77 Chieftan Way, Tallahassee, FL 32306, USA
[3] The Observatories of the Carnegie Institution for Science, 813 Santa Barbara Street, Pasadena, CA 91101, USA
[4] Carnegie Observatories, Las Campanas Observatory, Casilla 601, La Serena, Chile
[5] Homer L. Dodge Department of Physics and Astronomy, University of Oklahoma, 440 W. Brooks, Rm 100, Norman, OK 73019-2061, USA
[6] Hamburger Sternwarte, Gojenbergsweg 112, D-21029 Hamburg, Germany
[7] Department of Physics, The George Washington University, Corcoran Hall, 725 21st Street NW, Washington, DC 20052, USA
[8] George P. and Cynthia Woods Mitchell Institute for Fundamental Physics and Astronomy, Department of Physics and Astronomy, Texas A&M University, College Station, TX 77843, USA
[9] Institute of Space Sciences (ICE, CSIC), Campus UAB, Carrer de Can Magrans, s/n, E-08193 Barcelona, Spain
[10] Institut d'Estudis Espacials de Catalunya (IEEC), E-08034 Barcelona, Spain
[11] Astrophysics Research Institute, Liverpool John Moores University, IC2, Liverpool Science Park, 146 Brownlow Hill, Liverpool L3 5RF, UK
[12] Department of Physics and Astronomy, Aarhus University, Ny Munkegade 120, DK-8000 Aarhus C, Denmark
Received 2022 April 11; revised 2022 May 12; accepted 2022 May 22; published 2022 June 9

Abstract

We present early-time photometric and spectroscopic observations of the Type Ia supernova (SN Ia) 2021aefx. The early-time *u*-band light curve shows an excess flux when compared to normal SNe Ia. We suggest that the early excess blue flux may be due to a rapid change in spectral velocity in the first few days post explosion, produced by the emission of the Ca II H&K feature passing from the *u* to the *B* bands on the timescale of a few days. This effect could be dominant for all SNe Ia that have broad absorption features and early-time velocities over 25,000 km s^{-1}. It is likely to be one of the main causes of early excess *u*-band flux in SNe Ia that have early-time high velocities. This effect may also be dominant in the UV filters, as well as in places where the SN spectral energy distribution is quickly rising to longer wavelengths. The rapid change in velocity can only produce a monotonic change (in flux-space) in the *u* band. For objects that explode at lower velocities, and have a more structured shape in the early excess emission, there must also be an additional parameter producing the early-time diversity. More early-time observations, in particular early spectra, are required to determine how prominent this effect is within SNe Ia.

Unified Astronomy Thesaurus concepts: Type Ia supernovae (1728); Supernovae (1668); Time domain astronomy (2109)

1. Introduction

Type Ia supernovae (SNe Ia) are thought to come from the thermonuclear explosion of at least one carbon-oxygen white dwarf in a binary system (Whelan & Icko 1973; Iben & Tutukov 1984). Their peak luminosities are commonly used to measure luminosity distances to define the Hubble flow (e.g., Phillips 1993; Riess et al. 1998; Perlmutter et al. 1999). Yet, to date, determining the exact progenitor scenario (e.g., single degenerate versus double degenerate) or explosion mechanism (Chandrasekhar mass versus sub-Chandrasekhar mass) has eluded the community (e.g., Maoz et al. 2014; Blondin et al. 2017; Hoeflich et al. 2017; Ashall et al. 2018; Galbany et al. 2019; Jha et al. 2019).

In recent years high-cadence transient surveys such as the All-Sky Automated Survey for Supernovae (ASAS-SN; Shappee et al. 2014; Kochanek et al. 2017), the Asteroidal Terrestrial-impact Last Alert System (ATLAS; Tonry et al. 2018), the Distance less than 40 (DLT40),[13] and the Zwicky Transient Facility (ZTF; Bellm et al. 2019), have dramatically increased the number of SNe Ia caught within hours to days of explosion. The radiative transfer through the outer layers that can only be seen up to a few days after explosion allows us to model the explosion and measure the chemical properties of the progenitor system.

There have only been a handful of SNe Ia that have multiband photometry and were caught within hours of first light. A subset of these objects are thought to have early excess blue emission, two-component rising light curves, or blue bumps in their light curves. Some of these SNe are: SN 2012cg (Marion et al. 2016; Shappee et al. 2018), SN 2017cbv (Hosseinzadeh et al. 2017), ASAS-SN-18bt/2018oh (Dimitriadis et al. 2019; Shappee et al. 2019), SN 2019yvq (Miller et al. 2020; Tucker et al. 2021), and SN 2020hvf (Jiang et al. 2021). For a summary of SNe Ia with early excess light-curve emission, see Jiang et al. (2018). Another subset of SNe Ia have smooth rising light curves such as SN 2011fe (Nugent et al. 2011), ASAS-SN-14lp (Shappee et al. 2016), and SN 2015F (Cartier et al. 2017). Furthermore, the early-time color curves of SNe Ia have shown diversity (Stritzinger et al. 2018; Bulla et al. 2020).

[13] http://dark.physics.ucdavis.edu/dlt40/DLT40

The cause of the early-time light-curve diversity is unknown, but various effects have been proposed. These include: (1) the collision of the ejecta with a companion star in a single degenerate system (Marietta et al. 2000; Kasen 2010); (2) the presence of ^{56}Ni in the outer layer, which can be mixed out from the center of the explosion or produced in situ (Piro & Morozova 2016; Ni et al. 2022); or (3) the interaction of the ejecta with circumstellar material (Gerardy et al. 2007; Dragulin & Hoeflich 2016; Piro & Morozova 2016; Jiang et al. 2021).

However, to date, no work has been carried out on determining if rapidly changing spectral features can produce the observed diversity in the rising light curves. In this work, we quantify the effect that a rapidly changing spectral feature has on the fixed-filter early light curves. We use observations of SN 2021aefx as a test case. In Section 2 the data are presented, in Section 3 we discuss how the data are calibrated, in Section 4 the results are shown, and the discussion is presented in Section 5.

2. Data

2.1. Discovery

SN 2021aefx was discovered by the DLT40 transient survey on 2021 November 11 12:30:43.78 UT (MJD 59529.52) at 17.24 mag, with a last nondetection on 2021 November 6 07:52:17 UT (MJD 59524.33) at 19.35 mag. Both the discovery and last nondetection were in a clear filter (Valenti et al. 2021). SN 2021aefx was classified as a high-velocity SN Ia using a spectrum obtained ∼8 hr (2021 November 11 20:55:27 UT; MJD 59529.87) after discovery (Bostroem et al. 2021). ASAS-SN (Shappee et al. 2014; Kochanek et al. 2017) places tighter constraints on the last nondetection with a limiting 3σ observation of 17.70 mag in the g band on 2021 November 9 08:37:39 UT (MJD 59527.36). The host of SN 2021aefx (NGC 1566) has a heliocentric redshift of 0.0050 (Allison et al. 2014), which corresponds to a distance modulus of 31.43 ± 0.15 mag when corrected for the local peculiar motion of the Virgo, Great Attractor, and Shapley clusters (Mould et al. 2000). Alternatively, using the tip of the red giant branch (TRGB) produces a distance modulus of 31.27 ± 0.49 mag (Sabbi et al. 2018).

2.2. Photometry

Multiband (*uBVgri*) follow-up observations were initiated by the Precision Observations for Infant Supernovae Explosions (POISE; Burns et al. 2021) a day after discovery. The photometry was obtained on the 1 m Swope Telescope at the Las Campanas Observatory. Observations were acquired twice per night in order to look for small scale fluctuations in the light curve. The photometry was reduced and analyzed using the same methods outlined by Krisciunas et al. (2017) and Phillips et al. (2019). The uncertainties shown in Figure 1 are derived from the usual propagation of errors assuming Poisson statistics, as well as the uncertainty in the nightly zero-points derived from observations of standard stars (see Krisciunas et al. 2017). A further source of potential error that is not included is the contamination of host galaxy light. While visual inspection indicates this is likely very small, final photometry and errors will require observations of the host galaxy after the SN has faded. A log of the photometric observations can be found in Table 1. The early-time light curve is presented in the top panel of Figure 1. The middle panel in Figure 1 demonstrates that the rise is not well characterized by a simple constant-temperature fireball expansion $f \propto t^2$, which gives an invalid time of explosion that is after the discovery. However, there is no good reason why the $f \propto t^2$ should provide an exact match to the data (Nugent et al. 2011). A power law that allows the index to vary ($f \propto t^{3.34}$) fits the u-band rise better, but still underestimates the flux of the first three data points. In fact, the u-band light curve may be best described as having a two-component rise, which may be identified as early excess emission in the 2 days following discovery. For the

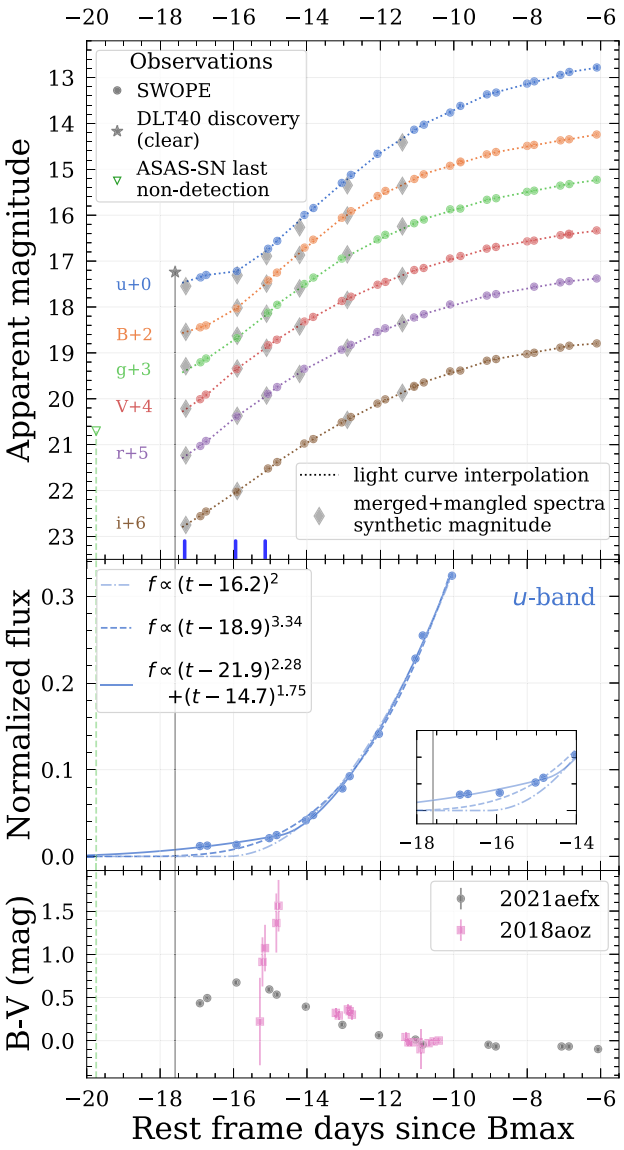

Figure 1. (Top): multiband photometric observations of SN 2021aefx. The ASAS-SN last nondetection and DLT40 discovery are indicated with open triangle and filled star, respectively. The dotted lines show the interpolation of the early-time light curves that are used for color correcting the spectra. The diamonds represent the synthetic magnitudes of integrating the mangled spectra described in Section 3. The vertical blue lines on the bottom mark the epochs of the observed spectra of SN 2021aefx. (Middle): power-law fits to the rising u-band light. The dashed–dotted line is the $f \propto t^2$ fit, the dashed line allows for the power-law index to vary, and the solid line is the two-component fit. (Bottom): the early-time $B-V$ color curves of SN 2021aefx and SN 2018aoz. Both SNe have an initial period where they turn red before becoming blue. The error bars are plotted but are smaller than the points. The plotted light- and color curves are corrected for Milky Way extinction.

Table 1
Swope e2v Optical Photometry of SN 2021aefx[a]

MJD	Phase[b]	*u*	*g*	*B*	*V*	*r*	*i*
59530.2	−16.9	17.39(0.02)	16.48(0.01)	16.24(0.01)	16.04(0.01)	16.05(0.01)	16.57(0.01)
59530.4	−16.7	17.34(0.04)	16.43(0.01)	16.15(0.01)	15.93(0.01)	15.94(0.01)	16.47(0.01)
59531.2	−15.9	17.26(0.02)	16.06(0.01)	15.71(0.01)	15.38(0.01)	15.41(0.01)	16.04(0.01)
59532.1	−15.0	16.77(0.02)	15.46(0.01)	15.15(0.01)	14.86(0.01)	14.91(0.01)	15.54(0.01)
59532.3	−14.8	16.60(0.02)	15.28(0.01)	14.98(0.01)	14.74(0.01)	14.77(0.01)	15.40(0.02)
59533.1	−14.0	16.03(0.02)	14.74(0.01)	14.53(0.01)	14.34(0.01)	14.37(0.01)	14.99(0.01)
59533.3	−13.8	15.88(0.02)	14.56(0.01)	14.39(0.01)	14.24(0.01)	⋯	14.90(0.01)
59534.1	−13.0	15.34(0.02)	14.09(0.01)	13.98(0.01)	13.90(0.01)	13.95(0.01)	14.53(0.01)
59534.3	−12.8	15.16(0.02)	13.94(0.01)	⋯	13.8(0.01)	13.85(0.01)	14.41(0.01)
59535.1	−12.0	14.70(0.02)	13.61(0.01)	13.56(0.01)	13.54(0.01)	13.57(0.01)	14.12(0.01)
59535.3	−11.8	⋯	13.50(0.01)	13.46(0.01)	13.48(0.01)	13.49(0.01)	14.03(0.01)
59536.1	−11.0	14.18(0.02)	13.24(0.01)	13.20(0.01)	13.22(0.01)	13.25(0.01)	13.75(0.01)
59536.3	−10.8	14.06(0.02)	13.14(0.01)	13.12(0.01)	13.18(0.01)	13.18(0.01)	13.66(0.01)
59537	−10.1	⋯	12.96(0.01)	⋯	12.97(0.01)	12.97(0.01)	13.42(0.01)
59537.1	−10.0	13.80(0.04)	⋯	12.90(0.01)	⋯	⋯	⋯
59537.3	−9.9	13.66(0.02)	12.87(0.01)	12.89(0.01)	12.92(0.01)	⋯	13.40(0.01)
59538.1	−9.1	13.40(0.02)	12.71(0.01)	12.69(0.01)	12.75(0.01)	12.77(0.01)	13.19(0.01)
59538.3	−8.9	13.36(0.02)	12.66(0.01)	12.66(0.01)	12.72(0.01)	12.74(0.01)	13.15(0.01)
59539.2	−8.0	13.17(0.02)	12.52(0.01)	12.52(0.01)	12.60(0.01)	⋯	13.04(0.01)
59539.3	−7.9	⋯	12.50(0.01)	⋯	12.58(0.01)	12.58(0.01)	⋯
59539.4	−7.8	13.12(0.02)	⋯	12.50(0.01)	⋯	⋯	13.01(0.01)
59540.1	−7.1	12.98(0.01)	12.40(0.01)	12.38(0.01)	12.46(0.01)	12.49(0.01)	12.90(0.01)
59540.3	−6.9	12.92(0.02)	12.38(0.01)	12.35(0.01)	12.44(0.01)	12.46(0.01)	12.86(0.01)
59541.1	−6.1	12.82(0.05)	12.27(0.01)	12.26(0.01)	12.36(0.01)	12.40(0.01)	12.81(0.01)

Notes.
[a] Magnitudes in the Swope+e2v natural system.
[b] Relative to the *B*-band maximum of 2021aefx at MJD = 59547.29.

two-component fit and the fireball model the 13 data points shown in the middle panel of Figure 1 are used in the fitting process. The two-component fit has six free parameters and a reduced χ^2 of 28. Whereas the fireball model had two free parameters and a reduced χ^2 of 664, and the one-component power-law fit has three free parameters and reduced χ^2 is 276. We note that the two-component rise in SN 2021aefx is different from the one seen in the Kepler filter for ASAS-SN-18bt (Shappee et al. 2019). This is because the Kepler filter covers a much larger wavelength range (∼4000–9000 Å). Therefore, in SN 2021aefx the effect likely comes from a different physical process.

A full detailed analysis of the later epochs of SN 2021aefx will be presented in a future paper. However, here we provide some important information about the SN for context. SN 2021aefx peaked at an apparent *B*-band magnitude of 11.99 ± 0.01 mag, and has a decline rate of $\Delta m_{15}(B) = 1.01 \pm 0.06$ mag.[14] This corresponds to an absolute *B*-band magnitude of -19.28 ± 0.49 mag, using the TRGB distance of $\mu = 31.27$ mag, and a foreground galactic extinction of $E(B-V)_{MW} = 0.01$ mag (Schlafly & Finkbeiner 2011). Throughout this work the data have been correct for foreground galactic extinction. This places it in the normal part of the luminosity width relation, and in a similar location to SN 2009ig, which has $M_B = -19.46 \pm 0.50$ mag and $\Delta m_{15}(B) = 0.90 \pm 0.07$ mag (Marion et al. 2013).

Furthermore, the $B-V$ color curve of SN 2021aefx has the unusual behavior where it starts red, and then turns blue within the first 2 days, see Figure 1. This is unlike any SN in the $B-V$ sample of Stritzinger et al. (2018), but is similar to SN 2018aoz. However, the evolution of SN 2018aoz is more extreme compared to SN 2021aefx. For SN 2018aoz this effect has been interpreted as enhanced line blanketing in the outer layers of the ejecta caused by iron group elements (Ni et al. 2022).

2.3. Spectroscopy

We present seven spectra of SN 2021aefx. Four were taken from the Transient Name Server database,[15] one was acquired using MIKE on the 6.5 m Magellan Clay Telescope, and two were obtained using IMACS on the 6.5 m Magellan Baade Telescope at the Las Campanas Observatory. The spectra were reduced using standard IRAF[16] packages following the method as described by Hamuy et al. (2006). A log of the spectra can be found in Table 2. The spectra are presented in Figure 2.

The earliest spectrum of SN 2021aefx (at −17.3 days[17]) was obtained during the early excess emission phase in the *u*-band light curve. This early-time spectrum shows high velocity and broad spectral features. Whereas, by −7.9 days the spectrum resembles a normal SN Ia. At this phase it is located between the core normal and broad line SNe in the branch diagram (Branch et al. 2009). At −17.3 days, the velocity of the absorption minimum of the Si II λ6355 feature reaches ∼30,000 km s^{-1} (see bottom right panel of Figure 3). Within 1.4 days, this velocity drops to ∼21,000 km s^{-1}. This deceleration is larger than other SNe Ia caught in these early stages, for example SN 2011fe

[14] $\Delta m_{15}(B)$ is the change in *B*-band magnitude between maximum light and 15 days past maximum.

[15] https://www.wis-tns.org/

[16] The Image Reduction and Analysis Facility (iraf) is distributed by the National Optical Astronomy Observatory, which is operated by the Association of Universities for Research in Astronomy, Inc., under cooperative agreement with the National Science Foundation.

[17] Throughout this work, all phases (in days) are provided relative to rest-frame *B*-band maximum.

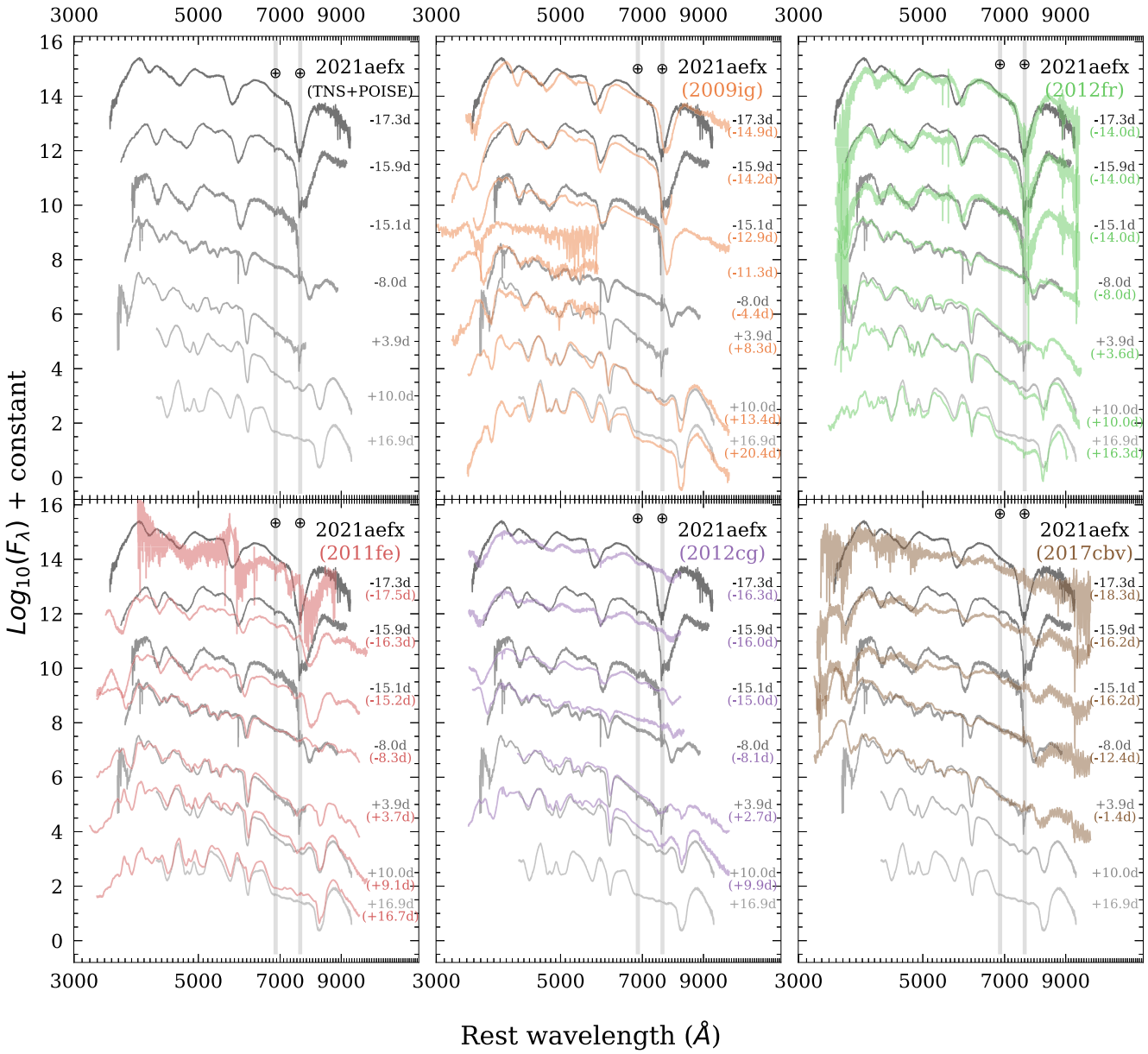

Figure 2. Spectra comparison of SN 2021aefx and a variety of other SNe Ia. SN 2021aefx is most similar to SNe 2009ig and 2012fr. Interestingly, the comparison also shows that 2021aefx is not the same as SN 2012cg or SN 2017cbv despite them having an early excess blue flux. Throughout this work, we use the spectra of SN 2009ig to fill in gaps in wavelength and phase.

Table 2
Journal of Spectroscopic Observations

UT Date	MJD	Phase[a] (day)	Telescope/Instrument	Source
2021-11-11	59529.87	−17.3	SALT + RSS	TNS
2021-11-13	59531.27	−15.9	NTT + EFOSC2	ePESSTO+
2021-11-14	59532.08	−15.1	Alpy600+35 cm R-C	TNS
2021-11-21	59539.29	−7.9	Clay + MIKE	POISE
2021-12-3	59551.21	3.9	Alpy600+35 cm R-C	TNS
2021-12-9	59557.35	10.0	Baade + IMACS	POISE
2021-12-16	59564.27	16.9	Baade + IMACS	POISE

Note.
[a] Relative to the *B*-band maximum of 2021aefx at MJD = 59547.29.

declined from 16,000 km s^{-1} to 13,000 km s^{-1} over similar epochs. In fact, at early times all of the spectral lines in SN 2021aefx are higher in velocity compared to SN 2011fe, as is seen in Figure 2.

Although it is apparent that there is diversity in the rising light curves of SNe Ia, few spectra have been obtained or analyzed during these early phases. SN 2021aefx is the first public example of an SN with an early excess *u*-band emission that also has high-velocity spectra in the early phases. Given that the velocity of the spectral lines rapidly decreases over the course of a few days, it is natural to ask the question: Could a rapid change in velocity of the ejecta produce the early excess *u*-band emission? For example, it could be the case that at early times the spectral features are so shifted to the blue that they

affect the broadband photometry. The blueshift may add flux to the *u* band. We investigate this further below. In fact, the sensitivity of broadband photometry to spectral features near the edges of the photometric bandpasses was noted as far back as Suntzeff et al. (1988) when comparing CTIO and SAAO *I*-band photometry, which could differ by 0.3 mag.

3. Constructing Spectrophotometric Data

While the spectra cover most of the *u* band, they do not cover the entire bandpass so careful consideration is warranted. Therefore, assumptions must be made about the nature of the spectral energy distribution in this region. In order to establish which objects have the same ionization state and line ratios, SN 2021aefx is compared to a range of SNe Ia that have early-time spectra. This is done to ensure that any extrapolation to the blue is made with an SN that has similar ejecta properties. At early times, 2021aefx does not resemble SN 2011fe, SN 2012cg, or SN 2017cbv, but is remarkably similar to SN 2012fr (Contreras et al. 2018) and SN 2009ig (Foley et al. 2012; Marion et al. 2013). Figure 2 shows these comparisons. The latter objects are SNe with high velocities and broad features at early times. For example, at ∼−15 days the pseudoequivalent width (pEW) of the Si II 6355 feature for SN 2021aefx, SN 2009ig, and SN 2012fr is larger than 150 Å, whereas the pEW of SN 2011fe is ∼100 Å. Conveniently, some early-time spectra of SN 2009ig extend into the blue and cover the whole wavelength range of the *u* band.

In order to extend the spectra of SN 2021aefx to cover the whole of the *u*-band region, we merge the blue part of the spectra of SN 2009ig onto the spectra of SN 2021aefx. However, before doing this, the spectra of SN 2009ig are matched to the closest phase of SN 2021aefx, and are then shifted in velocity to match the optical features of SN 2021aefx. The assumption made here is that if SNe Ia are very similar in the *BVgri* bands, they should also be similar in the *u* band. We do note that SNe that are optical twins might not always have similar mid- and far-UV flux. For example, SNe 2011fe and 2011by were spectroscopic twins in the optical but differed in the mid- and far-UV (Foley & Kirshner 2013; Graham et al. 2015). However, when the spectra are normalized in the 4000–5500 Å region at −10 days SNe 2011fe and 2011by only differ in *u*-band flux by 6%.

An example of the merged spectrum is presented in the top right panel of Figure 3. SN 2009ig does not have *u*-band photometry early enough to determine if it has an early excess blue flux. However, at the earliest time 96% of the *u*-band flux in the merged spectrum region comes from the data of SN 2021aefx, and only 4% comes from the added/merged data. To determine if the choice of SN for the merging process affects the results, we also ran the trial using SN 2011fe as the merged spectrum. Using SN 2011fe only 9% of the flux in the *u* band comes from SN 2011fe. Therefore, the merging process does not significantly affect our results.

The *merged* spectra are then color matched (also referred to as mangled) with the *uBVgri* bands to the observed photometry of SN 2021aefx (see the left panel of Figure 3). The color matching is done using the MANGLE function in the SuperNovae in object-oriented Python (SNooPy) program (Burns et al. 2011). Cubic splines were fit with control points located at the effective wavelengths of each filter. In addition, two "stabilizing" filters are introduced 100 Å to the blue of the bluest filter and to the red of the reddest filter. These extra control points are given the same flux as through the bluest and reddest filters, forcing the spline to have zero slope at the ends. Integrating the spectra through the *uBVgri* filters at each epoch correctly produces the observed light curve, as is seen in Figure 1.

4. The Effects of Rapidly Changing Velocity Profiles

Having established that the data set used in the analysis is spectrophotometric, we can then begin to explore if different velocity evolutions of the ejecta would produce changes in the early-time behavior of the light curve. The first approach is to study the effect of velocity on the *u*- and *B*-band photometry at a single epoch. In the top left panel of Figure 4, the −17.3 days spectra of SN 2021aefx are presented at various velocities, shifted by increments of 1000 km s^{-1}. Note that where we discuss the velocity shift, it is relative to the minimum of the Si II λ6355 feature. At each velocity shift the synthetic *u*- and *B*-band magnitudes are calculated.[18] The assumption made here is that the underlying chemical distribution and state of the spectra stay the same at every velocity (i.e., the ionization state and line ratios do not change), and only a wavelength shift is applied. The inlay in the figure demonstrates how the synthetic magnitude changes as a function of the velocity shift. Across a velocity range of 14,000 km s^{-1}, starting at the observations (30,000 km s^{-1}) and decreasing to 16,000 km s^{-1}, the synthetic *B* band stays constant. However, the synthetic *u* band drops by ∼1 mag. This demonstrates that, at a given time, spectra with higher velocities are likely to have brighter *u*-band magnitudes. The drop in flux is caused by the steepness of the spectrum across the *u* passband; specifically the emission component from the Ca II H&K feature is being redshifted from the *u*- to the *B* band as the velocity of the spectrum decreases. In the middle left panel of Figure 4 we also show the same velocity test carried out with the −14.2 days spectrum of SN 2009ig. The difference in the *u*-band magnitude between the low-velocity and high-velocity spectrum is 0.87 mag.

The next stage of the analysis is to determine if various velocity evolution pathways of the spectral time series significantly affect the rising flux of the SN. To do this, a range of velocity profiles was created between the evolution of SN 2021aefx and SN 2011fe; see the right panel of Figure 4. There is no significant difference between the low-velocity and high-velocity profiles in the *B* band; however there is a clear difference in the early *u*-band behavior. The shape of the rising light curve in *u* changes dramatically within the first few days between the high-velocity and low-velocity time series. The high-velocity time series produces an apparent early excess flux within the *u* band. If the different synthetic *u* bands are fit with a power law, the high-velocity time series requires a two-component power-law fit, whereas the low-velocity time series can be fit by a power law of $f \propto t^{7.7}$.

In the *u* band the low-velocity time series is 0.96 mag fainter than the high-velocity time series (i.e., the observations) at −17.3 days. The low-velocity time series rises smoothly and is similar to that of a "normal" SN Ia light curve. However, the high-velocity time series has an early excess flux in the *u* band. These results suggest that in this case, this excess flux is caused by line profiles shifting to shorter wavelengths. In particular, at early times the Ca II H&K emission is located within the *u* band

[18] It is important to note, that we are moving the spectra without moving the bandpass. In this case the zero-point does not need recalculating. However, if the bandpass was moved the zero-point would need recalculating.

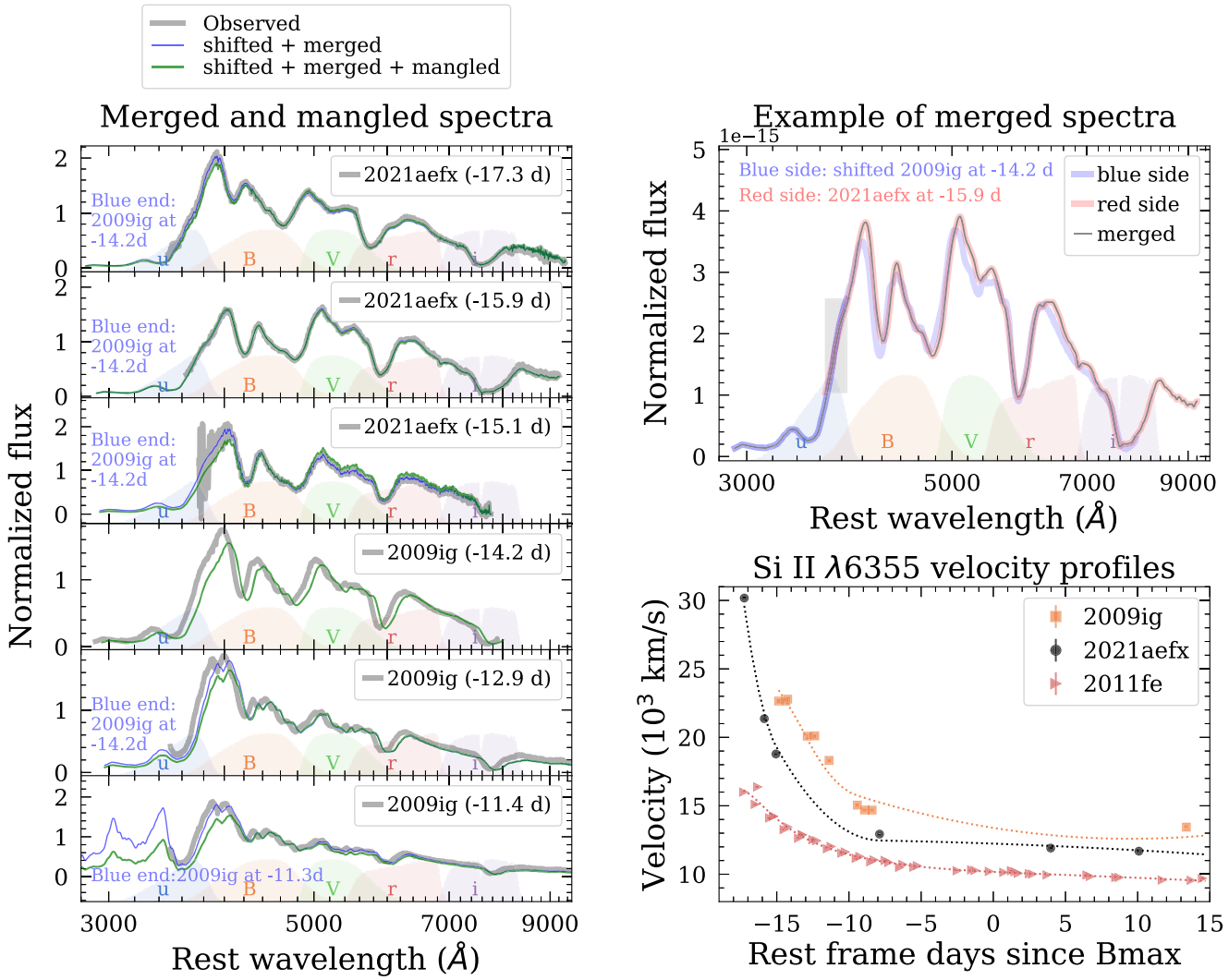

Figure 3. (Left): the six color-adjusted spectra chosen for this analysis, including three early spectra of SN 2021aefx and three spectra of SN 2009ig. The spectra are color matched to the observed photometry of SN 2021aefx. (Top right): an example of the merging process between SN 2021aefx and SN 2009ig. Before the merging process, the spectra of SN 2009ig are shifted in velocity to match the velocity of SN 2021aefx at the same phase. The gray shade marks the overlapping region used to match the flux scale. (Bottom right): Velocity profiles of the minimum of the Si II λ6355 feature in SN 2011fe, SN 2009ig, and SN 2021aefx.

for SNe that have high velocities, but not for SNe Ia that have lower velocities. An example of how different velocity gradients affect the underlying opacity can be seen in Figures 1 and 2 of Hoeflich et al. (1993).

Many SNe Ia that have early excess emission in the u band also have excess emission at mid-UV wavelengths. SN 2021aefx does not have early-time UV observations available; therefore we cannot test the effects directly for this object. However, as a test case we use the -13.3 days spectrum of SN 2011fe to determine if the rapid drop in spectral flux can also produce early excess flux in the UV (see the bottom left panel of Figure 4). For SN 2011fe the Swift UVM2 and UVW1 magnitudes drop by 0.74 mag and 0.41 mag, respectively, over a velocity change from 30,000 to 13,000 km s^{-1}, but stay constant in the B band. We note that the HST spectra do not go far enough into the blue to test that UVw2 filter. While the spectrum of SN 2011fe is taken at a different time compared to the phase where the blue early excess is seen, it acts as proof of a concept. Generally, if there is a large slope in the flux across a passband then a rapid change in the velocity of the profiles can cause an additional structure within the rising light curves. However, we note that there is another effect of velocities at these mid-UV wavelength ranges, since the opacity in this region is almost entirely dominated by line blanketing due to iron group elements (DerKacy et al. 2020). Increasing velocity tends to depress the flux in the UV since the increased velocity leads to an increased effective opacity in this region (Wang et al. 2012), which our assumptions neglect. This effect is clearly seen in SNe 2017erp and 2021fxy (J. M. DerKacy et al. 2022, in preparation).

Finally, we tested how the u-band flux changes with spectra of SNe Ia that do not have broad spectral features (see the bottom left panel of Figure 4). By using the spectrum of SN 2011fe at -13.3 days, the minimum of the features were artificially increased in velocity to 30,000 km s^{-1}. The change in u-band magnitude between the high-velocity spectrum and low-velocity spectrum is 0.5 mag and demonstrates that velocity has an important effect. However, the effect of the velocity shift is smaller in SN 2011fe than in SN 2021aefx because the features in SN 2011fe are narrower. For SN 2021aefx with its broader features, the short wavelength edge of the absorption of Ca II H&K will eat into the emission region of the adjacent shorter wavelength features, producing excess line blanketing and further reducing the flux in the region. Therefore, we conclude

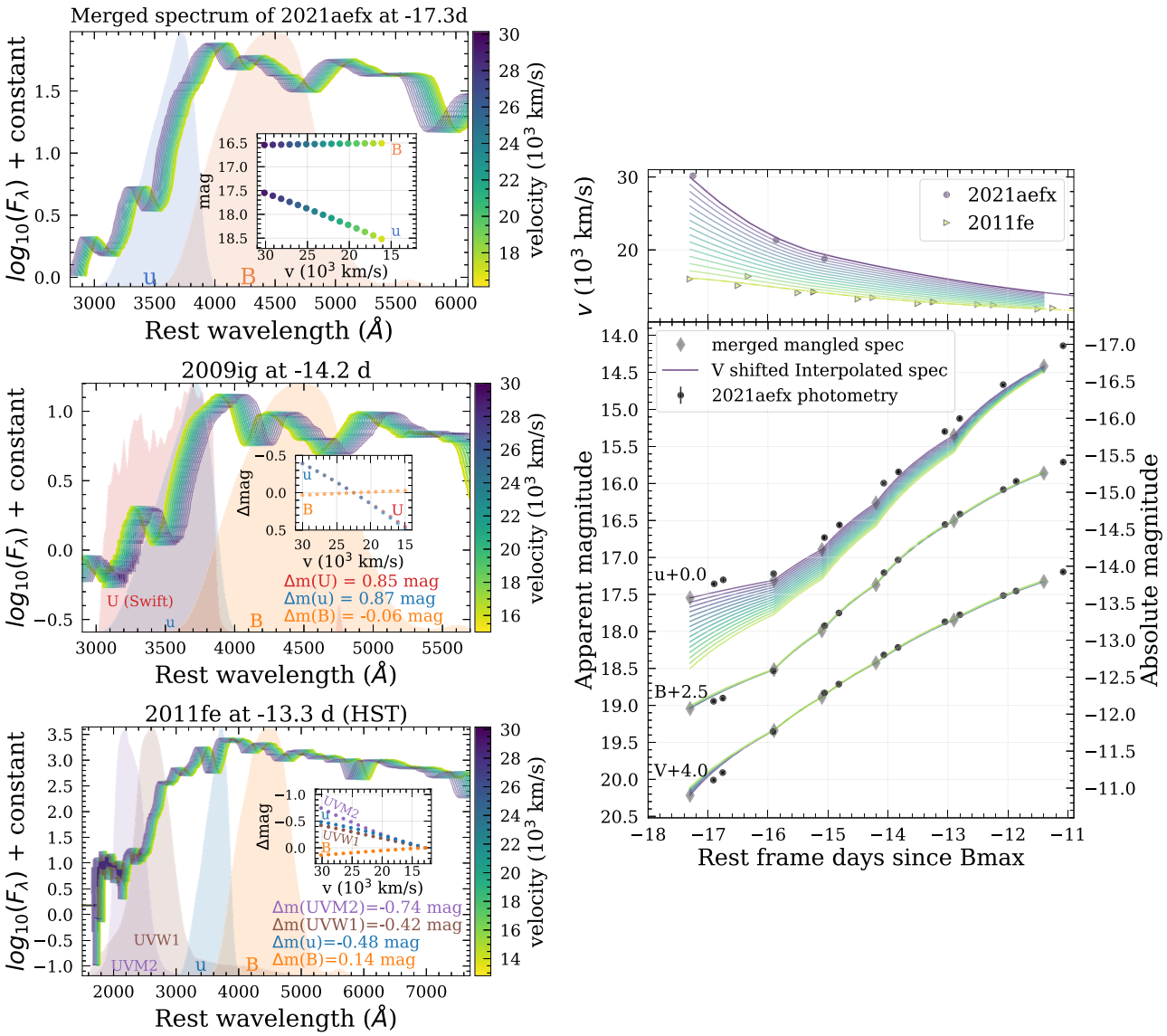

Figure 4. (Top left): illustration of how changing the velocity of the −17.3 days spectrum can affect the *u*-band and *B*-band synthetic magnitudes. The scale on the right denotes the velocity shift, where 30,000 km s^{-1}, is the velocity of the observed spectra. (Middle left): similar to the top left panel but with the spectrum of SN 2009ig at −14.2 days (Foley et al. 2012). In this panel we also present the magnitude change in the swift *U* band. (Bottom left): similar to the top left panel but with the spectrum of SN 2011fe at −13.3 days (Mazzali et al. 2014) taken with the Hubble Space Telescope. Interestingly, the drop in magnitude effect is larger in the UVM2 band than the *u* band, on top of this the drop in UVW1 is similar in magnitude to that of the *u* band. (Right): the synthetic light curves (bottom panel) of the spectrophotometric time series with a different velocity evolution. The upper panel shows the chosen velocity evolution for this analysis. These are velocity profiles between SN 2021aefx and SN 2011fe. The *u*-band light curves show significant changes in magnitudes and shape for various velocity profiles, whereas the *B* band remains relatively constant. At −17.3 days the *u* band changes by 0.96 mag between the high-velocity and low-velocity models. Conversely, the *B* band only changes by 0.03 mag at the same epoch.

the effect seen in SN 2021aefx is produced by both the high velocity and the broadness of the spectral features.

After the submission of this work Hosseinzadeh et al. (2022) presented early-time observations of SN 2021aefx. They showed that an early-time open-filter light curve of SN 2021aefx had a structure that may be interpreted as an early excess flux. However, the early-time shoulder in the DLT40 open filter is different from the early excess blue flux see in the *u* and UV filters, but is similar in shape to our *V*-band light curves. In this work we concentrate on the nature of the *u* and UV early flux as this shows the largest early excess flux. Our work here demonstrates that for this particular SN, the Doppler effect accounts for most of the excess in the UV and *u* bands leaving little room for additional effects. Therefore, any model fitting of early SNe Ia must consider the effect of Doppler shift on the *u* and UV light curves.

5. Discussion

We provide a cautionary tale that the early-time diversity seen in *u*-band light curves of SNe Ia can be caused, in part, by the rapid change in the velocity of the Ca II H+K feature. This prediction is only true for SNe Ia that have early-time high-velocity and broad spectral profiles (i.e., objects that have expansion velocities higher than 25,000 km s^{-1} in the earliest phases).

The effect is produced by the Ca II H&K emission rapidly passing from the *u* band and into the *B* band causing a change in flux and change in slope of the *u*-band light curve. The rapid change in velocity can produce various *u*-band light curves that monotonically increase, but it cannot explain all of the early-time diversity in SNe Ia light curves, such as the more complex bump-like shapes seen in objects like SN 2017cbv (Hosseinzadeh et al.

2017). In fact, given the fact that SN 2017cbv has ejecta velocities lower than $\approx$25, 000 km s^{-1} we would not expect the effect discussed here to be the dominant cause. Furthermore, in normal velocity SNe Ia such as SN 2011fe this effect is also not expected to be large. However, for a light curve of an object such as SN 2012cg (Marion et al. 2016) the effect discussed here may be able to explain the early blue excess flux. Only spectra taken in this earliest phase would reveal if the lines are of high enough velocity or broad enough for the effect to be dominant.

The work here should also provide a word of warning that if one is to interpret the *u*-band flux between observations at different telescopes of the same SN, a precise knowledge of the transmission function is required otherwise variation between *u*-band flux may be due to whether the blue edge of the Ca II H&K feature is in the bandpass or not.

To fully understand the effects that a rapid change in velocity has on the light curve requires high-cadence spectral data that cover the whole of the rest-frame *u* band, and are obtained within hours after the explosion. Future follow-up observations of transients should ensure that the whole wavelength range is observed.

Finally, although this work may not explain all of the diversity within early SNe Ia light curves, our results should be carefully considered when interpreting physical meaning from SNe Ia that have early-time high ejecta velocities and early excess UV and *u*-band light curves.

C.A. and B.J.S. are supported by NSF grants AST-1907570, AST-1908952, AST-1920392, and AST-1911074. M.D.S. is funded in part by an Experiment grant (No. 28021) from the Villum FONDEN, and by a project 1 grant (No. 8021-00170B) from the Independent Research Fund Denmark (IRFD). P.H. acknowledges support by National Science Foundation (NSF) grant AST- 1715133. E.B. and J.D. are supported in part by NASA grant 80NSSC20K0538. This work has been generously supported by the National Science Foundation under grants AST-1008343, AST-1613426, AST-1613455, and AST1613472. This paper includes data gathered with the 6.5 meter Magellan Telescopes located at the Las Campanas Observatory, Chile. We would like to thank the technical staff for constant support for observations on the Swope telescope. The early-time spectrum that was critical for this analysis came from SALT through Rutgers University time via program 2021-1-MLT-007 (PI: Jha). L.G. acknowledges financial support from the Spanish Ministerio de Ciencia e Innovación (MCIN), the Agencia Estatal de Investigación (AEI) 10.13039/501100011033, and the European Social Fund (ESF) "Investing in your future" under the 2019 Ramón y Cajal program RYC2019-027683-I and the PID2020-115253GA-I00 HOSTFLOWS project, from Centro Superior de Investigaciones Científicas (CSIC) under the PIE project 20215AT016, and the program Unidad de Excelencia María de Maeztu CEX2020-001058-M.

ORCID iDs

C. Ashall https://orcid.org/0000-0002-5221-7557
J. Lu https://orcid.org/0000-0002-3900-1452
B. J. Shappee https://orcid.org/0000-0003-4631-1149
C. R. Burns https://orcid.org/0000-0003-4625-6629
E. Y. Hsiao https://orcid.org/0000-0003-1039-2928
S. Kumar https://orcid.org/0000-0001-8367-7591
N. Morrell https://orcid.org/0000-0003-2535-3091
M. M. Phillips https://orcid.org/0000-0003-2734-0796
M. Shahbandeh https://orcid.org/0000-0002-9301-5302
E. Baron https://orcid.org/0000-0001-5393-1608
K. Boutsia https://orcid.org/0000-0003-4432-5037
P. J. Brown https://orcid.org/0000-0001-6272-5507
J. M. DerKacy https://orcid.org/0000-0002-7566-6080
L. Galbany https://orcid.org/0000-0002-1296-6887
P. Hoeflich https://orcid.org/0000-0002-4338-6586
K. Krisciunas https://orcid.org/0000-0002-6650-694X
A. L. Piro https://orcid.org/0000-0001-6806-0673
M. D. Stritzinger https://orcid.org/0000-0002-5571-1833
N. B. Suntzeff https://orcid.org/0000-0002-8102-181X

References

Allison, J. R., Sadler, E. M., & Meekin, A. M. 2014, MNRAS, 440, 696
Ashall, C., Mazzali, P. A., Stritzinger, M. D., et al. 2018, MNRAS, 477, 153
Bellm, E. C., Kulkarni, S. R., Graham, M. J., et al. 2019, PASP, 131, 018002
Blondin, S., Dessart, L., Hillier, D. J., & Khokhlov, A. M. 2017, MNRAS, 470, 157
Bostroem, K. A., Jha, S. W., Randriamampandry, S., et al. 2021, TNSCR, 2021
Branch, D., Chau Dang, L., & Baron, E. 2009, PASP, 121, 238
Bulla, M., Miller, A. A., Yao, Y., et al. 2020, ApJ, 902, 48
Burns, C., Hsiao, E., Suntzeff, N., et al. 2021, ATel, 14441, 1
Burns, C. R., Stritzinger, M., Phillips, M. M., et al. 2011, AJ, 141, 19
Cartier, R., Sullivan, M., Firth, R. E., et al. 2017, MNRAS, 464, 4476
Contreras, C., Phillips, M. M., Burns, C. R., et al. 2018, ApJ, 859, 24
DerKacy, J. M., Baron, E., Branch, D., et al. 2020, ApJ, 901, 86
Dimitriadis, G., Foley, R. J., Rest, A., et al. 2019, ApJL, 870, L1
Dragulin, P., & Hoeflich, P. 2016, ApJ, 818, 26
Foley, R. J., Challis, P. J., Filippenko, A. V., et al. 2012, ApJ, 744, 38
Foley, R. J., & Kirshner, R. P. 2013, ApJL, 769, L1
Galbany, L., Ashall, C., Höflich, P., et al. 2019, A&A, 630, A76
Gerardy, C. L., Meikle, W. P. S., Kotak, R., et al. 2007, ApJ, 661, 995
Graham, M. L., Foley, R. J., Zheng, W., et al. 2015, MNRAS, 446, 2073
Hamuy, M., Folatelli, G., Morrell, N. I., et al. 2006, PASP, 118, 2
Hoeflich, P., Hsiao, E. Y., Ashall, C., et al. 2017, ApJ, 846, 58
Hoeflich, P., Mueller, E., & Khokhlov, A. 1993, A&A, 268, 570
Hosseinzadeh, G., Sand, D. J., Lundqvist, P., et al. 2022, arXiv:2205.02236
Hosseinzadeh, G., Sand, D. J., Valenti, S., et al. 2017, ApJL, 845, L11
Iben, I. J., & Tutukov, A. V. 1984, ApJS, 54, 335
Jha, S. W., Maguire, K., & Sullivan, M. 2019, NatAs, 3, 706
Jiang, J.-a., Doi, M., Maeda, K., & Shigeyama, T. 2018, ApJ, 865, 149
Jiang, J.-a., Maeda, K., Kawabata, M., et al. 2021, ApJL, 923, L8
Kasen, D. 2010, ApJ, 708, 1025
Kochanek, C. S., Shappee, B. J., Stanek, K. Z., et al. 2017, PASP, 129, 104502
Krisciunas, K., Contreras, C., Burns, C. R., et al. 2017, AJ, 154, 211
Maoz, D., Mannucci, F., & Nelemans, G. 2014, ARA&A, 52, 107
Marietta, E., Burrows, A., & Fryxell, B. 2000, ApJS, 128, 615
Marion, G. H., Brown, P. J., Vinkó, J., et al. 2016, ApJ, 820, 92
Marion, G. H., Vinko, J., Wheeler, J. C., et al. 2013, ApJ, 777, 40
Mazzali, P. A., Sullivan, M., Hachinger, S., et al. 2014, MNRAS, 439, 1959
Miller, A. A., Magee, M. R., Polin, A., et al. 2020, ApJ, 898, 56
Mould, J. R., Huchra, J. P., Freedman, W. L., et al. 2000, ApJ, 529, 786
Ni, Y. Q., Moon, D.-S., Drout, M. R., et al. 2022, NatAs, 6, 568
Nugent, P. E., Sullivan, M., Cenko, S. B., et al. 2011, Natur, 480, 344
Perlmutter, S., Aldering, G., Goldhaber, G., et al. 1999, ApJ, 517, 565
Phillips, M. M. 1993, ApJL, 413, L105
Phillips, M. M., Contreras, C., Hsiao, E. Y., et al. 2019, PASP, 131, 014001
Piro, A. L., & Morozova, V. S. 2016, ApJ, 826, 96
Riess, A. G., Filippenko, A. V., Challis, P., et al. 1998, AJ, 116, 1009
Sabbi, E., Calzetti, D., Ubeda, L., et al. 2018, ApJS, 235, 23
Schlafly, E. F., & Finkbeiner, D. P. 2011, ApJ, 737, 103
Shappee, B. J., Holoien, T. W. S., Drout, M. R., et al. 2019, ApJ, 870, 13
Shappee, B. J., Piro, A. L., Holoien, T. W. S., et al. 2016, ApJ, 826, 144
Shappee, B. J., Piro, A. L., Stanek, K. Z., et al. 2018, ApJ, 855, 6
Shappee, B. J., Prieto, J. L., Grupe, D., et al. 2014, ApJ, 788, 48
Stritzinger, M. D., Shappee, B. J., Piro, A. L., et al. 2018, ApJL, 864, L35
Suntzeff, N. B., Hamuy, M., Martin, G., Gomez, A., & Gonzalez, R. 1988, AJ, 96, 1864
Tonry, J. L., Denneau, L., Heinze, A. N., et al. 2018, PASP, 130, 064505
Tucker, M. A., Ashall, C., Shappee, B. J., et al. 2021, ApJ, 914, 50
Valenti, S., Sand, D. J., Wyatt, S., et al. 2021, TNSTR, 2021
Wang, X., Wang, L., Filippenko, A. V., et al. 2012, ApJ, 749, 126
Whelan, J. I., & Icko, J. 1973, ApJ, 186, 1007